Supporting Information for

Alkoxy Radical Bond Scissions Explain the Anomalously Low Secondary Organic Aerosol and Organonitrate Yields from α-Pinene + NO_3

Theo Kurtén,[a] Kristian H. Møller,[b] Tran B. Nguyen,[c] Rebecca H. Schwantes,[d,e] Pawel K. Misztal,[f] Luping Su,[g] Paul O. Wennberg,[d,h] Juliane L. Fry,[i] Henrik G. Kjaergaard*[,b]*

a) Department of Chemistry, University of Helsinki, P.O. Box 55, FI-00014 Helsinki, Finland
b) Department of Chemistry, University of Copenhagen, Universitetsparken 5, DK-2100 Copenhagen Ø, Denmark
c) Department of Environmental Toxicology, University of California – Davis, Davis, California 95616, USA
d) Division of Geological and Planetary Sciences, California Institute of Technology, 1200 E. California Blvd, Pasadena, California 91125, USA
e) Current affiliation: National Center for Atmospheric Research, Boulder, Colorado, 80301, USA
f) Department of Environmental Science, Policy, & Management, University of California – Berkeley, Berkeley, California 94720, USA
g) School of Marine and Atmospheric Sciences, Stony Brook University, Stony Brook, NY, USA
h) Division of Engineering and Applied Science, California Institute of Technology, 1200 E. California Blvd, Pasadena, California 91125, USA
i) Chemistry Department, Reed College, Portland, Oregon 97202, USA

Corresponding Authors:

*Theo Kurtén, theo.kurten@helsinki.fi, Tel: +358 50 526 0123

*Henrik G. Kjaergaard, hgk@chem.ku.dk, Tel +45 3532 0334

OUTLINE OF SI

S1. Computational details.

S2. Thermodynamics of the alkyl and peroxy radicals.

S3. The minor NO_3 addition pathway in α-pinene (NO_3 addition to tertiary carbon).

S4. Δ^3-carene + NO_3 nitrooxy-peroxy radical isomers.

S5. Reaction kinetic modeling of alkyl radical ring-breaking (opening of the 4-membered ring) in the α-pinene - NO_3 adduct.

S6. H-shift reaction rates for nitrooxy-peroxy radicals formed in the nitrate oxidation of α-pinene and Δ^3-carene.

S7. Thermodynamics of nitrooxy-alkoxy formation from reaction of nitrooxy-peroxy radicals with HO_2.

S8. Transition states for all isomers for the alkoxy radical bond scission reactions in the α-pinene + NO_3 and Δ^3-carene + NO_3 systems.

S9. Alkoxy radical bond scission reactions in the α-pinene + OH and Δ^3-carene + OH systems.

S10. Transition states and energetics for reaction **R6** (bond scission in the keto-nitrooxy-alkyl radical formed in the Δ-carene + NO_3 system by reaction **R5b**).

S11. Detailed description of experimental instrumentation.

S12. Alkoxy bond breaking reactions in isoprene-derived nitrooxy-alkoxy radicals.

S1. Computational details

The computational methods employed in this study follow, to a large extent, those investigated and tested H-shift reactions of smaller molecules, in a recent manuscript,[1] but with necessary modification due to both the much larger computational challenge associated with the monoterpenes and the different nature of some of the reactions. The reaction rate constants are calculated within a multi-conformer transition state theory framework (MC-TST), which requires identification of all possible conformers.[1-2]

Systematic configurational sampling was first carried out with the Spartan'14 program[3] using the MMFF force-field (with the FFHINT keyword set to the correct neutral charge on all radical centers), followed by B3LYP/6-31+G(d) optimizations and frequency calculations on all unique structures using Gaussian 09 Rev. D.01.[4] In the force-field stage, transition states were treated using constrained optimizations, with the constraints determined from B3LYP/6-31+G(d) transition state optimizations on an arbitrary conformer. The constrained parameters were the C-C bond lengths of the bond being broken for all ring-breaking (bond scission) reactions, and the C-O, O-H and H-C bond lengths of the reacting groups for H-shifts. For the bond scission reactions, further transition state conformers were sampled by manually elongating the bond being broken in each of the located reactant conformers to a length corresponding to that in an arbitrary transition state conformer. All MMFF conformer searches in Spartan were started from a B3LYP/6-31+G(d) optimized geometry of an arbitrary conformer. Transition state conformer searches were followed by B3LYP/6-31+G(d) constrained optimizations (with the constraints as described above), followed by transition state optimizations. Duplicate structures were removed as described in Møller *et al*.[1]

Due to the large size of the monoterpene + NO_3 systems (16 non-hydrogen atoms in the first-generation peroxy radicals), CCSD(T) energy corrections needed for accurate absolute barrier heights could not be performed for the peroxy or alkoxy radicals, and the ωB97X-D/aug-cc-pVTZ frequency calculations were also prohibitively expensive. For this reason, most reactions were treated by re-optimizing only the lowest-energy and the lowest zero-point corrected energy conformers (these were the same except for a few cases) from the B3LYP calculations at the ωB97X-D/aug-cc-pVTZ level. For the nitrooxy-alkyl radical bond scission in the α-pinene + NO_3 system, CCSD(T)-F12/VDZ-F12 energy corrections could be computed (albeit at great expense). These were performed with the Molpro 2012.1 program. In accordance with recommendations,[5] these F12 calculations were carried out using the geminal Slater exponent β=0.9 (gem_beta=0.9). In the ωB97X-D calculations, the ultrafine integration grid was used, with default settings for convergence criteria and other parameters. For some systems, the ωB97X-D/aug-cc-pVTZ frequency calculation did not converge using these settings. In those cases, the additional keywords Integral(Acc2e=12) and CPHF(grid=ultrafine) were used. Test calculations indicate that these additional key words have a negligible effect on the electronic energies and frequencies. We find that for the alkoxy radical, the calculations may converge to an electronic state that is not the lowest. The stability of the state located can be checked using the keyword Stable.

For the alkoxy radical bond scission reactions, which turned out to be the key difference between the α-pinene + NO_3 and Δ^3-carene + NO_3 systems, all conformers within 2 kcal/mol in electronic energy of the lowest-energy conformer at the B3LYP level were re-optimized at the ωB97X-D/aug-cc-pVTZ level. This cut-off has been shown to be cost-effective.[1] While the lack of coupled-cluster energy corrections, and the extremely low barriers of some of the reactions, prevents us from calculating quantitatively accurate absolute reaction rate constants, our main focus here is on relative rates of different reaction routes, for which the applied approach is sufficient.

We have calculated the rates using either multi-conformer transition state theory (MC-TST) or lowest energy conformer transition state theory (LC-TST) as described in Møller et al.[1] For the H-shift reactions, tunneling was treated using the Eckart model. The other reactions studied have imaginary frequencies well below 1000***i*** cm^{-1}, and tunneling can thus be neglected. For computational reasons, product energies for the Eckart tunneling were estimated only at the B3LYP/6-31+G(d) level. The reverse barrier needed for the Eckart calculation was then obtained by combining the ωB97X-D/aug-cc-pVTZ forward barrier (reactant – transition state zero-point corrected energy difference) with the B3LYP reaction energy (reactant-product zero-point corrected energy difference). We note that the tunneling correction computed with this approach corresponds to an upper limit for the Eckart tunneling, as the true barrier height for the actual tunneling process is likely lower (since the reactants and products connected to the transition state are unlikely to be the lowest-energy reactants and products). See Møller *et al.*[1] for further discussion on this topic. For some of the H-shift reactions arising from nitrate carbon atoms, NO_2 loss followed promptly, and no local minimum corresponding to a hydroperoxy nitrate alkyl radical could be found. In these cases, the reverse barrier was qualitatively estimated from an intrinsic reaction co-ordinate (IRC) scan.

S2. Thermodynamics of the alkyl and peroxy radicals

Computing reliable reaction rate coefficients for barrierless (or low-barrier) radical + alkene and O_2 + radical addition reactions requires a combination of high-level (coupled cluster) quantum chemical methods and variational transition state theory. Such a combination is computationally far too expensive for the systems studied here. However, the branching ratios of the addition reactions are mainly controlled by the stabilities of the various radical centers (e.g. secondary vs. tertiary), and so can be estimated based on the reaction thermodynamics, which are much easier to compute. Accordingly, we have computed the reaction energies for the addition reactions relevant to this study (**R1a**, **R1b** and **R2** in Scheme 1 of the main article): the addition of NO_3 (and also OH) to α-pinene and Δ^3-carene, and the addition of O_2 to the radicals formed from the first addition reaction. The results are presented in tables S1 and S2. As expected, addition to the secondary carbon (leading to a radical center on the tertiary carbon) is favored, with the difference being larger for NO_3 addition than for OH addition. The NO_3 addition energies to both alkenes are around 20 kcal/mol, while the OH addition energies are around 30 kcal/mol, reflecting the well-known relative reactivities of the two radicals. The O_2 addition reactions are also somewhat more exothermal for the OH-alkyl radicals than for the NO_3-alkyl radicals.

Table S1. Reaction energies (zero-point corrected ωB97X-D/aug-cc-pVTZ electronic energies, based on B3LYP/6-31+G(d) conformational sampling) for addition of NO_3 and OH to α-pinene and Δ^3-carene.

Reaction	NO_3 or OH addition site and R,S isomer of adduct	Reaction energy (kcal/mol)
α-pinene + NO_3	Secondary C, R	-21.77
α-pinene + NO_3	Secondary C, S	-22.93
α-pinene + NO_3	Tertiary C, R	-19.99
α-pinene + NO_3	Tertiary C, S	-19.71
Δ^3-carene + NO_3	Secondary C, R	-17.89
Δ^3-carene + NO_3	Secondary C, S	-20.54
Δ^3-carene + NO_3	Tertiary C, R	-16.50
Δ^3-carene + NO_3	Tertiary C, S	-17.74
α-pinene + OH	Secondary C, R	-30.45
α-pinene + OH	Secondary C, S	-31.16
α-pinene + OH	Tertiary C, R	-31.39
α-pinene + OH	Tertiary C, S	-31.49
Δ^3-carene + OH	Secondary C, R	-28.52
Δ^3-carene + OH	Secondary C, S	-29.11
Δ^3-carene + OH	Tertiary C, R	-28.23
Δ^3-carene + OH	Tertiary C, S	-28.43

Table S2. Reaction energies (zero-point corrected ωB97X-D/aug-cc-pVTZ electronic energies, based on B3LYP/6-31+G(d) conformational sampling) for addition of O_2 to the NO_3 and OH adducts of α-pinene and Δ^3-carene.

Reaction	NO_3 or OH addition site and R,S isomer of radical adduct	R, S isomer of O_2 adduct	Reaction energy (kcal/mol)
α-pinene-NO_3 + O_2	Secondary C, R	R	-23.33
α-pinene-NO_3 + O_2	Secondary C, R	S	-21.48
α-pinene-NO_3 + O_2	Secondary C, S	R	-19.99
α-pinene-NO_3 + O_2	Secondary C, S	S	-23.08
α-pinene-NO_3 + O_2	Tertiary C, R	R	-20.37
α-pinene-NO_3 + O_2	Tertiary C, R	S	-22.24
α-pinene-NO_3 + O_2	Tertiary C, S	R	-21.31
α-pinene-NO_3 + O_2	Tertiary C, S	S	-19.87
Δ^3-carene-NO_3 + O_2	Secondary C, R	R	-27.38
Δ^3-carene-NO_3 + O_2	Secondary C, R	S	-27.09
Δ^3-carene-NO_3 + O_2	Secondary C, S	R	-21.60
Δ^3-carene-NO_3 + O_2	Secondary C, S	S	-24.34
Δ^3-carene-NO_3 + O_2	Tertiary C, R	R	-25.33
Δ^3-carene-NO_3 + O_2	Tertiary C, R	S	-24.67
Δ^3-carene-NO_3 + O_2	Tertiary C, S	R	-24.15
Δ^3-carene-NO_3 + O_2	Tertiary C, S	S	-25.15
α-pinene-OH + O_2	Secondary C, R	R	-27.28
α-pinene-OH + O_2	Secondary C, R	S	-25.77
α-pinene-OH + O_2	Secondary C, S	R	-24.37
α-pinene-OH + O_2	Secondary C, S	S	-26.66
α-pinene-OH + O_2	Tertiary C, R	R	-25.57
α-pinene-OH + O_2	Tertiary C, R	S	-25.77
α-pinene-OH + O_2	Tertiary C, S	R	-24.63
α-pinene-OH + O_2	Tertiary C, S	S	-25.03
Δ^3-carene-OH + O_2	Secondary C, R	R	-27.80
Δ^3-carene-OH + O_2	Secondary C, R	S	-28.79
Δ^3-carene-OH + O_2	Secondary C, S	R	-26.48
Δ^3-carene-OH + O_2	Secondary C, S	S	-30.17
Δ^3-carene-OH + O_2	Tertiary C, R	R	-28.90
Δ^3-carene-OH + O_2	Tertiary C, R	S	-27.49
Δ^3-carene-OH + O_2	Tertiary C, S	R	-28.79
Δ^3-carene-OH + O_2	Tertiary C, S	S	-29.82

S3. The minor NO_3 addition pathway in α-pinene (NO_3 addition to tertiary carbon)

To understand the yield of pinonaldehyde and the hydroperoxy nitrate following NO_3 addition to the tertiary carbon (**R1b** in Scheme 1 of the main manuscript) we need to consider the yield of alkoxy radicals in the reaction of the peroxy radicals with HO_2 and, for the channel leading to alkoxy radicals, which C-C bond is broken. As discussed in the main body of the manuscript, reaction of HO_2 with the peroxy radical following addition of NO_3 at the tertiary carbon may have a substantially lower alkoxy yield than for the equivalent reaction following addition at the secondary carbon; neither our calculations nor laboratory experiments, however, provide a significant constraint. In order to investigate whether the same preference for scission of the C-C(ONO_2) bond occurs if the alkoxy radical is produced following addition of NO_3 to the tertiary carbon (by reactions analogous to **R2**, **R4** and **R5a/b** in Scheme 1 of the main manuscript), we investigated the competitive bond scission reactions of the nitrooxy-alkoxy radicals formed via this channel. Hydrogen shifts of nitrooxy-peroxy radicals formed in this channel were not studied, as the same chemical features (lack of accessible hydrogens, steric strain, strongly bound hydrogens) that make them extremely slow in the major addition channel (see section S6) are present also in the minor channel.

For computational reasons, only the lowest zero-point corrected energy transition states (for each of the four R,S isomer with respect to the NO_3 and O_2 group positions) from the B3LYP conformer sampling were treated at the ωB97X-D/aug-cc-pVTZ level. The energy difference between the transition states for breaking the C-C(H_2) bond (analogous to reaction **R5b**) and the C-C(ONO_2) bond (analogous to reaction **R5a**) varied between 1.7 and 2.2 kcal/mol for the four different R,S isomers, with the transition state for breaking the C-C(ONO_2) bond always being lower in energy. This implies a branching ratio on the order of 1:20 in favor of pinonaldehyde formation, in agreement with results for the major NO_3 addition channel (Table 1 in the main text).

S4. Δ^3-carene + NO_3 nitrooxy-peroxy radical isomers

The lowest-energy conformers of the four isomers of the peroxy radicals formed in the NO_3-iniated oxidation of Δ^3-carene are shown in Figure S1. Using the R,S notation, the R,R and S,S isomers have the peroxy and nitrate groups on opposite sides of the ring, while the R,S and S,R isomers have them on the same side. The same naming convention applies to the alkoxy radicals formed from the peroxy radicals by bimolecular reactions.

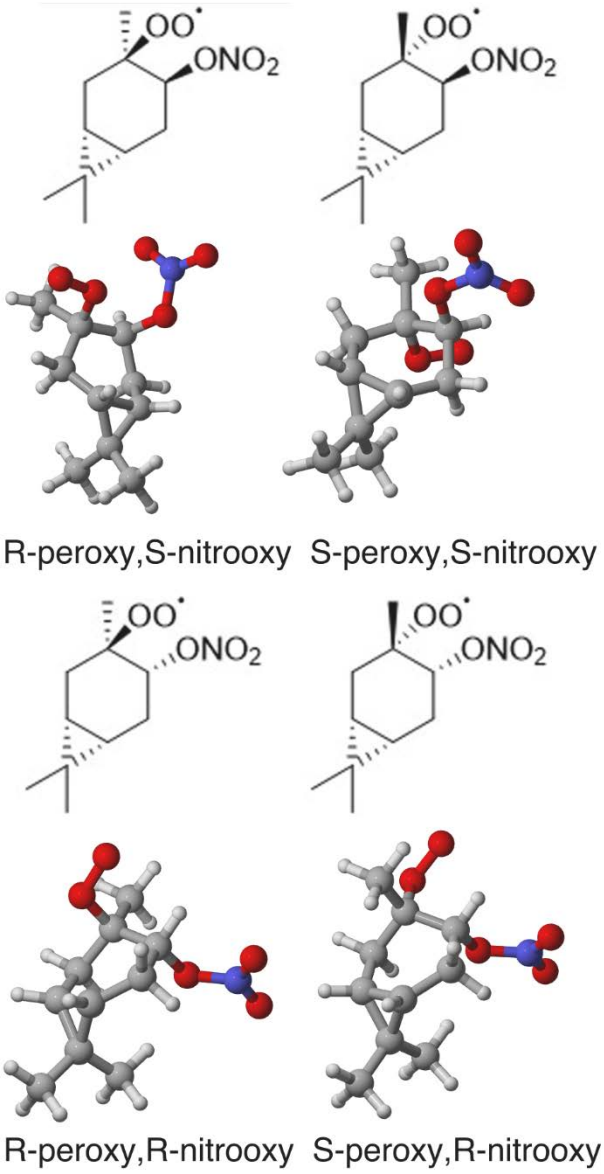

Figure S1. Structures of the four different isomers of the nitrooxy-peroxy radical formed in the oxidation of Δ^3-carene by NO_3, assuming initial radical addition to the secondary carbon atom. The S,S isomer is lowest in energy. Color coding: gray=C, white=H, red=O, blue=N.

S5. Reaction kinetic modeling of alkyl radical ring-breaking (opening of the 4-membered ring) in the α-pinene - NO_3 adduct

The competition between bond scission (ring-breaking to open the 4-membered ring) and O_2-addition in the nitrate adduct of α-pinene (**R2** and **R3** in scheme 1 in the main manuscript) was modelled using the Master Equation Solver for Multi Energy-well Reactions (MESMER)[6] to assess the product distribution between the two pathways. The modeling was carried out for both the R and S isomers of the nitrate adduct (nitrooxy alkyl radical) following addition to form the tertiary radical. The quantum chemical data used in the modeling is calculated at the ωB97X-D/aug-cc-pVTZ level for the lowest energy conformer of each species. The transition states for the alkyl radical ring-breaking reactions are shown in Figure S2, and the potential energy of the system in Figure S3. The zero-point corrected energy barrier for the bond scission at the ωB97X-D/aug-cc-pVTZ is 14.7 kcal/mol for both isomers. CCSD(T)-F12a/VDZ-F12 single-point energy calculations were performed on the lower-energy S-isomer. Combined with the ωB97X-D/aug-cc-pVTZ zero-point energy corrections, these yielded a barrier of 13.9 kcal/mol, indicating that the error of the ωB97X-D barrier is likely on the order of 1-2 kcal/mol.

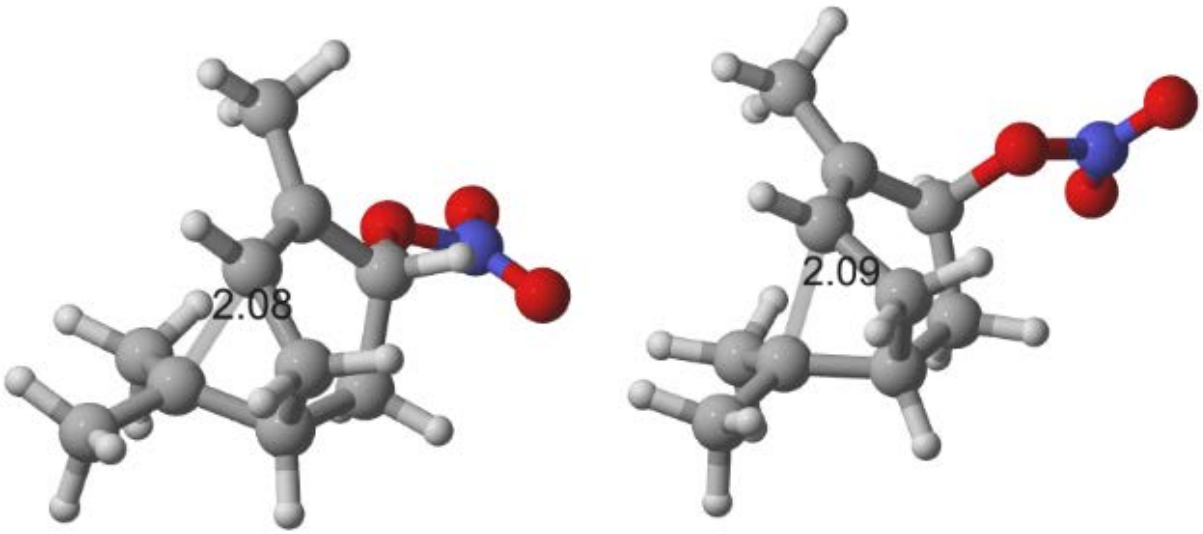

Figure S2. Lowest-energy transition states for the bond scission (ring-breaking) reactions of the nitrooxy-alkyl radicals formed in the addition of NO_3 to the secondary carbon atom of α-pinene (reaction R3 in Scheme 1 of the main text). The left-hand structure is the "R" and the right-hand structure the "S" isomer with respect to the $–ONO_2$ group. The C-C distance of the bond being broken is given in Ångström. Color coding as in Figures 1 and S1.

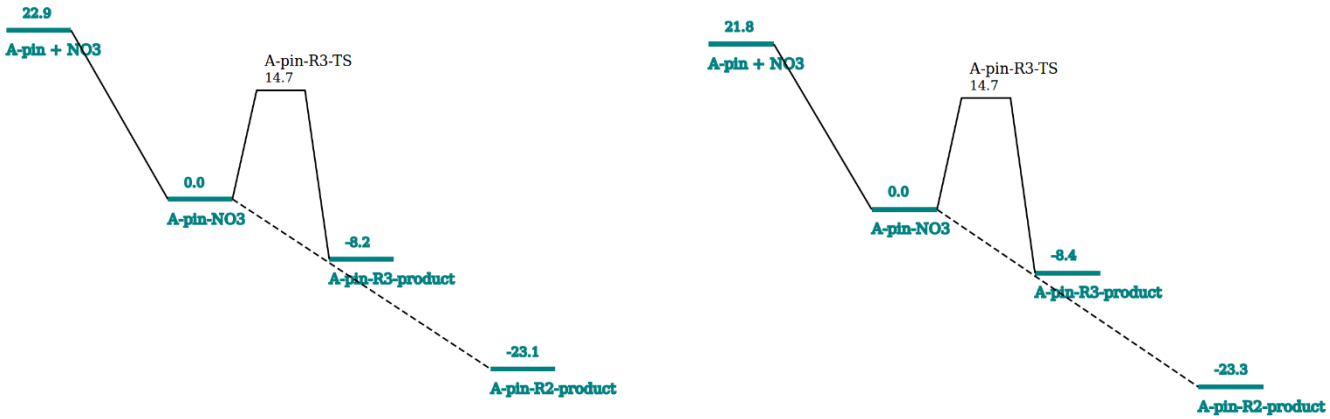

Figure S3. Potential energy surfaces used in the MESMER modeling for the α-pinene + NO_3 system, with formation of the S-nitrooxy (left) and R-nitrooxy (right) alkyl radicals from the α-pinene-NO_3 reaction. All energies are zero-point corrected ωB97X-D/aug-cc-pVTZ electronic energies in kcal/mol. The names of the structures refer to the reactions given in Scheme 1 in the main manuscript.

Molecular nitrogen (N_2) is used as the bath gas with Lennard-Jones parameters of ε = 91.85 K and σ = 3.919 Å.[7] For the α-pinene derived species, Lennard-Jones parameters of ε = 600 K and σ = 6.5 Å were used, as previously done in the modelling of similar α-pinene oxidation products.[8] The exponential-down collisional energy transfer model[9] was used with ΔE_{down} values of 225 cm^{-1}, as previously used with N_2 as the bath gas.[8, 10]

For the MesmerILT calculation of the NO_3 addition, the recommended Arrhenius pre-exponential factor of 1.2×10^{-12} cm^3 $molecule^{-1}$ s^{-1} was used,[11] but with an activation energy of zero rather than the recommended negative activation energy, which is not meaningful for elementary reactions. A modified Arrhenius parameter of -0.5 was used. The MESMER model was initiated with a large concentration of nitrate radicals (10^{18} molecule cm^{-3}, with nitrate set as the excess reactant) in order to form the nitrooxy-alkyl radical with a realistic energy distribution early on in the simulation. Note that the nitrate concentration affects only the rate at which the nitrooxy-alkyl radical is formed, and has no effect on its subsequent fate, or the product distribution (yield). For the O_2-addition to the nitrate-adduct, the Arrhenius parameters used are: a pre-exponential factor of 6×10^{-12} $cm^3molecule^{-1}s^{-1}$, an activation energy of 0 kcal/mol, and a modified Arrhenius parameter of -0.5. A number density of O_2 of 5.34×10^{18} molecules cm^{-3} was used in accordance with sea level values of the U.S. Standard Atmosphere 1962. Unlike the nitrate concentration, the absolute value of the oxygen concentration is important for the simulation.

For the bond scission reaction, for which a transition state could be located, the simple RRKM formalism was used. All simulations were carried out with a N_2 bath gas pressure of 1 atm = 760 Torr and the temperature range of 270-300 K was tested in steps of 10 K. An energy grain size of 15 cm^{-1} was used with a span of energy grains up to 50 k_bT above the highest stationary point.

For all simulations (on the ωB97X-D/aug-cc-pVTZ potential energy surface) the steady-state yield of the ring-opened product (A-pin-R3-product in Figure S3) was less than 1%. Very similar results were obtained for the S and R α-pinene-NO_3 adducts at the highest temperature (300 K) and a decreasing yield was found with decreasing temperature for both systems. Using the CCSD(T)-F12 barrier of 13.9 kcal/mol for the ring breaking of the S isomer increases the yield of the ring-opened

product to about 2 % at 300 K. These simulations thus suggest that bond scission leading to opening of the 4-membered ring is a negligible pathway for α-pinene + NO_3.

A sensitivity study conducted at 300 K shows that, as expected, the calculated mole fractions are sensitive mainly to the barrier for the bond scission, and to a much smaller degree, the energy of NO_3 addition. With a 2 kcal/mol decrease in the barrier for bond scission (i.e. with a barrier height about 1 kcal/mol lower than that indicated by the CCSD(T)-F12 single-point energy calculation) and a 2 kcal/mol increase in the energy of the NO_3 addition reaction, the mole fraction of the ring-opened product increases to around 12%, but bond scission still represents a minor channel. As a final test (run with a coarser grain of 100 cm^{-1} and energy grains up to 30 k_bT above the highest stationary point) we independently changed by ±50%: the Arrhenius pre-factors of the two addition reactions; the Lennard-Jones parameters of the α-pinene derived species; or the ΔE_{down} values. We found that the product distribution is quite insensitive to these values, with a maximum yield of the ring-opened product of less than 3%.

S6. H-shift reaction rates for nitrooxy-peroxy radicals formed in the nitrate oxidation of α-pinene and Δ^3-carene

The B3LYP/6-31+G(d) – level barriers and MC-TST rate constants for H-shifts of all accessible hydrogen atoms of all isomers of the nitrooxy-peroxy radicals formed in the nitrate oxidation of α-pinene and Δ^3-carene (assuming initial radical addition to the secondary carbon atom, to form a tertiary nitrooxy-alkyl radical) are shown in Table S3. For the initial identification of the fastest H-shift for each conformer, approximate Eckart tunneling corrections were computed assuming a thermoneutral reaction (i.e. reactant and product energies equal). The product energy was then computed for the fastest H-shift. In cases where the conformer with fastest rate depended on inclusion of tunneling or not, both reactions were tested at the ωB97X-D/aug-cc-pVTZ level, with tunneling calculated based on B3LYP product energies. The final ωB97X-D/aug-cc-pVTZ H-shift rates are given in Table S4, with the corresponding transition states shown in Figure S4.

Table S3. Barriers (zero-point corrected transition state - reactant electronic energy differences) and MC-TST reaction rate coefficients (at 298.15 K) computed at the B3LYP/6-31+G(d) level for all possible (accessible) hydrogen shift reactions for the nitrooxy-peroxy radicals formed in the nitrate oxidation of α-pinene and Δ^3-carene, assuming initial radical addition to the secondary carbon atom.

Peroxy radical isomer	Type of H-shift	Barrier (kcal/mol)	Rate coefficient without tunneling (s^{-1})	Rate coefficient with approx. tunneling (s^{-1})
R-peroxy,S-nitrooxy from α-pinene	1,5 CH_2 (on C_4 ring)	24.1	1.9×10^{-6}	2.6×10^{-5}
	1,5 CH_2 (on C_6 ring)	43.0	3.2×10^{-20}	3.7×10^{-16}
	1,4 CH_3	35.2	1.6×10^{-14}	2.5×10^{-9}
	1,4 CH (on C_6&C_4 rings)	35.9	3.2×10^{-15}	1.3×10^{-10}
S-peroxy,S-nitrooxy from α-pinene	1,4 CH(ONO_2)	31.1	1.2×10^{-11}	2.6×10^{-6}
	1,5 CH_2 (on C_6 ring)	48.6	1.6×10^{-24}	2.2×10^{-18}
	1,6 CH_3	25.3	2.5×10^{-7}	5.0×10^{-6}
	1,4 CH_3	35.9	1.1×10^{-14}	1.6×10^{-9}
	1,4 CH (on C_6&C_4 rings)	37.1	1.3×10^{-15}	7.6×10^{-11}
R-peroxy,R-nitrooxy from α-pinene	1,4 CH(ONO_2)	30.0	1.3×10^{-10}	2.6×10^{-5}
	1,5 CH_2 (on C_4 ring)	24.7	7.6×10^{-7}	1.8×10^{-5}
	1,5 CH_2 (on C_6 ring)	51.1	2.7×10^{-26}	2.5×10^{-19}
	1,4 CH_3	35.7	1.2×10^{-14}	2.5×10^{-9}
	1,4 CH (on C_6&C_4 rings)	36.7	2.2×10^{-15}	1.3×10^{-10}
S-peroxy,R-nitrooxy from α-pinene	1,5 CH_2 (on C_6 ring)	46.9	4.3×10^{-23}	8.4×10^{-18}
	1,6 CH_3	25.8	1.0×10^{-7}	1.2×10^{-6}
	1,4 CH_3	35.8	7.7×10^{-15}	1.2×10^{-9}
	1,4 CH (on C_4 ring)	37.3	4.8×10^{-16}	3.4×10^{-11}

Table S3 cont. Barriers (zero-point corrected transition state - reactant electronic energy differences) and MC-TST reaction rate coefficients (at 298.15 K) computed at the B3LYP/6-31+G(d) level for all possible (accessible) hydrogen shift reactions for the nitrooxy-peroxy radicals formed in the nitrate oxidation of α-pinene and Δ^3-carene, assuming initial radical addition to the secondary carbon atom.

R-peroxy,S-nitrooxy from Δ^3-carene	1,4 CH_3	34.6	1.0×10^{-13}	2.1×10^{-8}
	1,4 CH_2 (on C_6 ring)	30.5	8.3×10^{-11}	6.3×10^{-6}
	1,5 CH (on C_3 ring)	32.6	1.4×10^{-12}	2.6×10^{-9}
S-peroxy,S-nitrooxy from Δ^3-carene	1,4 CH_3	35.8	7.6×10^{-15}	7.7×10^{-10}
	1,4 CH_2 (on C_6 ring)	28.1	4.5×10^{-9}	2.7×10^{-5}
	1,4 $CH(ONO_2)$	31.7	2.8×10^{-11}	1.2×10^{-6}
	1,5 CH (on C_3 ring)	28.8	5.6×10^{-10}	3.9×10^{-7}
R-peroxy,R-nitrooxy from Δ^3-carene	1,4 CH_3	36.9	2.4×10^{-15}	5.7×10^{-10}
	1,4 CH_2 (on C_6 ring)	33.3	9.8×10^{-13}	7.0×10^{-8}
	1,4 $CH(ONO_2)$	31.4	6.3×10^{-11}	9.3×10^{-6}
	1,5 CH (on C_3 ring)	33.2	6.1×10^{-13}	1.0×10^{-9}
	1,5 CH_2 (on C_6 ring)	28.8	9.1×10^{-10}	2.9×10^{-6}
S-peroxy,R-nitrooxy from Δ^3-carene	1,4 CH_3	37.3	1.7×10^{-15}	5.4×10^{-10}
	1,4 CH_2 (on C_6 ring)	32.8	1.5×10^{-12}	3.0×10^{-8}
	1,4 $CH(ONO_2)$	39.8	4.6×10^{-18}	1.7×10^{-11}
	1,7 CH_3	24.2	9.0×10^{-7}	1.1×10^{-4}

Table S4. Barriers (zero-point corrected transition state - reactant electronic energy differences), Eckart tunneling corrections and reaction rate coefficients (at 298.15 K) computed at the ωB97X-D/aug-cc-pVTZ level for the fastest H-shifts calculated at the B3LYP/6-31+G(d) level. Identification of the fastest H-shift for each isomer, as well as estimates of the reverse reaction barrier needed for the tunneling correction, are based on B3LYP/6-31+G(d) calculations Reaction rates are computed using LC-TST including the tunneling correction.

Peroxy radical isomer	Type of fastest H-shift	Barrier (kcal/mol)	Eckart tunneling correction	Rate coefficient s^{-1}
α-pinene R-peroxy, S-nitrate	1,5 CH_2 (on C_4 ring)	24.0	12	6.8×10^{-5}
α-pinene S-peroxy, S-nitrate	1,6 CH_3	25.6	23	3.0×10^{-6}
α-pinene R-peroxy, R-nitrate	1,5 CH_2 (on C_4 ring)	25.2	6.8	5.1×10^{-7}
α-pinene R-peroxy, R-nitrate	1,4 $CH(ONO_2)$	30.56	5.8×10^{4}	3.9×10^{-6}
α-pinene S-peroxy, R-nitrate	1,6 CH_3	25.7	25	6.4×10^{-6}
Δ^3-carene R-peroxy, S-nitrate	1,4 CH_2 (on C_6 ring)	30.7	4.1×10^{4}	4.6×10^{-6}
Δ^3-carene S-peroxy, S-nitrate	1,4 CH_2 (on C_6 ring)	29.0	5.3×10^{3}	6.7×10^{-6}
Δ^3-carene R-peroxy, R-nitrate	1,5 CH_2 (on C_6 ring)	30.1	3.0×10^{3}	4.4×10^{-7}
Δ^3-carene R-peroxy, R-nitrate	1,4 $CH(ONO_2)$	32.4	2.4×10^{4}	2.6×10^{-7}
Δ^3-carene S-peroxy, R-nitrate	1,7 CH_3	25.7	64	1.5×10^{-5}

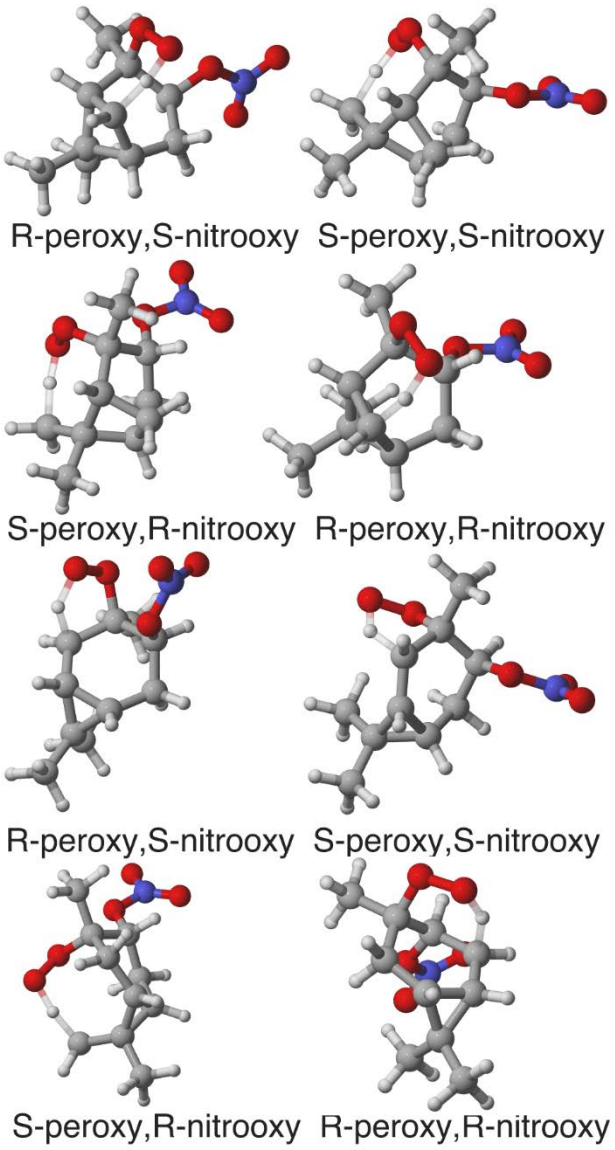

Figure S4. Lowest-energy H-shift transition state (optimized at the ωB97X-D/aug-cc-pVTZ level) found for each of the four structural isomers of the nitrooxy-peroxy radicals formed in the NO_3-initiated oxidation of α-pinene (top four) and Δ^3-carene (bottom four), assuming initial radical addition to the secondary carbon atom. See Table S4 for corresponding energies and rates. Color coding as in Figures 1 and S1.

S7. Thermodynamics of nitrooxy-alkoxy formation from reaction of nitrooxy-peroxy radicals with HO_2

For the nitrooxy- or hydroxyl-peroxy radicals formed by addition of NO_3 or OH to form the tertiary radical, followed by addition of O_2, we have investigated the thermodynamics of the bimolecular reaction with HO_2 to form alkoxy radicals (RO), O_2 and OH (reaction **R4a** in Schemes 1 and 2 in the main manuscript, with HO_2 as the bimolecular reaction partner). We have computed the Gibbs free energy of reaction at 298.15 K and 1 atm reference pressure. The results are shown in Table S5. For the alkoxy radicals, for which multiple ωB97X-D/aug-cc-pVTZ conformers had been calculated, the values correspond to the lowest Gibbs free energy conformers at the ωB97X-D/aug-cc-pVTZ level of theory.

Table S5. Reaction Gibbs free energies for the reaction of the nitrooxy-peroxy radical, formed by NO_3 or OH addition to the secondary carbon, reacting with HO_2 to form nitrooxy-alkoxy radical, O_2 and OH radicals. Reaction free energies are computed by subtracting the free energies of the reactants from those of the products.

Peroxy radical isomer	Gibbs free energy of reaction (kcal/mol)
α-pinene R-peroxy, S-nitrooxy	-4.1
α-pinene S-peroxy, S-nitrooxy	-3.4
α-pinene R-peroxy, R-nitrooxy	-1.4
α-pinene S-peroxy, R-nitrooxy	-5.2
Δ^3-carene R-peroxy, S-nitrooxy	-6.4
Δ^3-carene S-peroxy, S-nitrooxy	-4.0
Δ^3-carene R-peroxy, R-nitrooxy	-2.3
Δ^3-carene S-peroxy, R-nitrooxy	-3.4
α-pinene R-peroxy, S-hydroxyl	-4.6
α-pinene S-peroxy, S- hydroxyl	-1.9
α-pinene R-peroxy, R-hydroxyl	-0.45
α-pinene S-peroxy, R-hydroxyl	-6.7
Δ^3-carene R-peroxy, S-hydroxy	-5.0
Δ^3-carene S-peroxy, S-hydroxyl	-2.1
Δ^3-carene R-peroxy, R-hydroxyl	-2.4
Δ^3-carene S-peroxy, R- hydroxy l	-4.7

S8. Transition states for all isomers for the alkoxy radical bond scission reactions in the α-pinene + NO_3 and Δ^3-carene + NO_3 systems

The lowest-energy transition states of the bond scission reactions described in Table 1 of the main manuscript are shown in Figures S5 and S6.

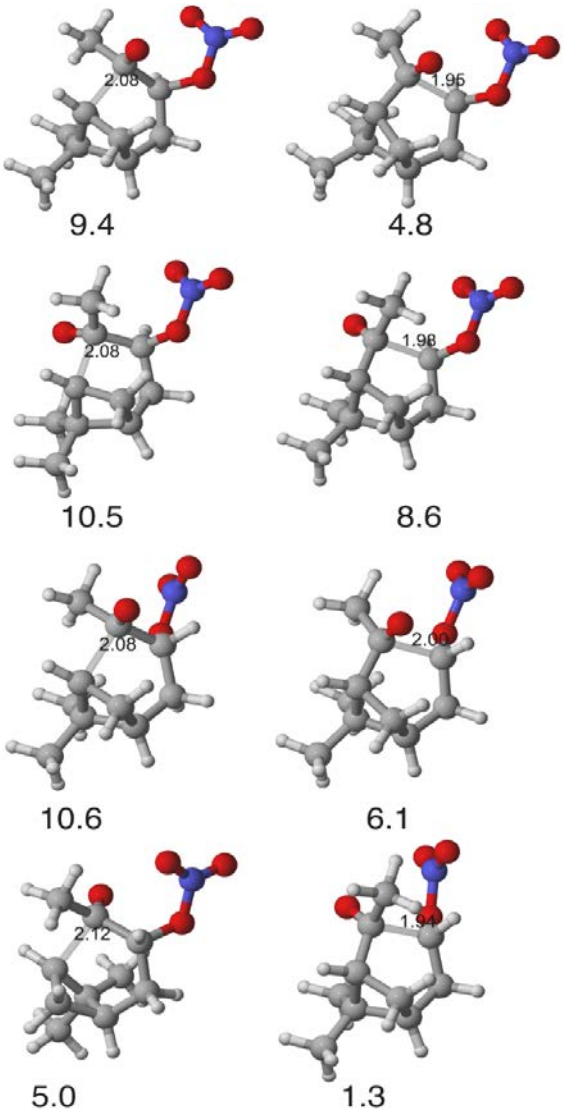

Figure S5. Lowest-energy transition states (at the ωB97X-D/aug-cc-pVTZ level) for the bond scission reactions (**R5a/b** in Scheme 1) of the four isomers of the nitrooxy-alkoxy radicals formed in the α-pinene + NO_3 reaction, assuming initial radical addition to the secondary carbon atom. The reaction barrier (transition state – reactant energy difference, zero-point corrected electronic energy) in kcal/mol is given under each structure, and the C-C distance of the bond being broken is given in Ångström. Left column: transition states for breaking the C-C(H) bond (**R5b**); Right column: transition states for breaking the C-C(ONO_2) bond (**R5a**). Top row: R-alkoxy, S-nitrate isomers; second row: S-alkoxy, S-nitrate isomers; third row: R-alkoxy, R-nitrate isomers; bottom row: S-alkoxy, R-nitrate isomers. Color coding as in Figure 1 & S1.

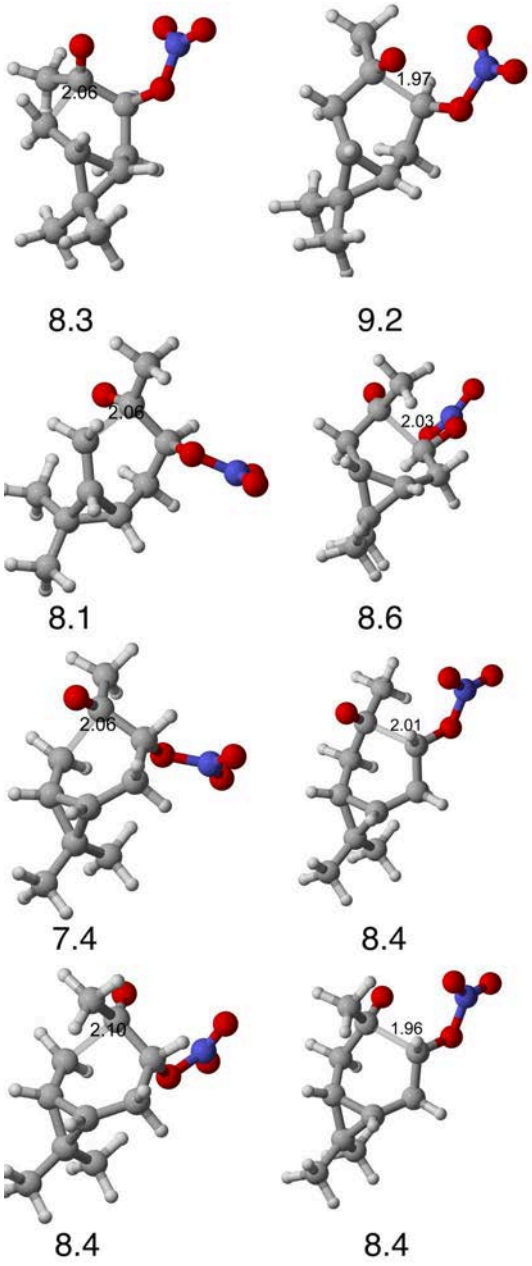

Figure S6. Lowest-energy transition states (at the ωB97X-D/aug-cc-pVTZ level) for the bond scission reactions (**R5a/b** in Scheme 2) of the four isomers of the nitrooxy-alkoxy radicals formed in the Δ^3-carene + NO_3 reaction, assuming initial radical addition to the secondary carbon atom. The reaction barrier (transition state – reactant energy difference, zero-point corrected electronic energy) in kcal/mol is given under each structure, and the C-C distance of the bond being broken is given in Ångström. Left column: transition states for breaking the C-C(H_2) bond (**R5b**); Right column: transition states for breaking the C-C(ONO_2) bond (**R5a**). Top row: R-alkoxy, S-nitrate isomers; second row: S-alkoxy, S-nitrate isomers; third row: R-alkoxy, R-nitrate isomers; bottom row: S-alkoxy, R-nitrate isomers. Color coding as in Figure 1 & S1.

S9. Alkoxy radical bond scission reactions in the α-pinene + OH and Δ^3-carene + OH systems

Data for the alkoxy ring-breaking reactions (C-C bond scissions, analogous to **R5a/b** in Schemes 1 and 2 of main manuscript) of all four hydroxyl alkoxy radical isomers formed in the α-pinene + OH and Δ^3-carene + OH systems (assuming initial OH addition to the secondary carbon atom) are given in Table S6.

Table S6. Barriers (zero-point corrected transition state-reactant electronic energy differences) and reaction rate coefficients (298.15 K) computed at the ωB97X-D/aug-cc-pVTZ level for the bond scission reactions of the hydroxyl alkoxy radicals formed in the α-pinene + OH and Δ^3-carene + OH reactions (assuming initial OH radical addition to the secondary carbon atom, and bimolecular reaction of hydroxyl peroxy radicals to form hydroxyl alkoxy radicals). Reaction rates are computed using multiconformer transition-state theory.

Alkoxy radical isomer	Barrier for breaking C-C(OH) bond, analogous to **R5a** in Schemes 1 or 2 (kcal/mol)	MC-TST Rate coefficient (s^{-1})	Barrier for breaking C-C(H) or C-C(H_2) bond, analogous to **R5b** in Schemes 1 or 2 (kcal/mol)	MC-TST Rate coefficient (s^{-1})
α-pinene R-alkoxy, S-hydroxyl	3.5	2.4×10^{10}	9.0	2.9×10^{6}
α-pinene S- alkoxy, S-hydroxyl	2.9	5.3×10^{10}	9.8	7.9×10^{5}
α-pinene R- alkoxy, R-hydroxyl	1.9	2.4×10^{11}	11.0	1.3×10^{5}
α-pinene S- alkoxy, R-hydroxyl	5.3	1.9×10^{9}	11.4	5.8×10^{4}
Δ^3-carene R- alkoxy, S-hydroxyl	3.8	1.4×10^{10}	5.4	5.0×10^{8}
Δ^3-carene S- alkoxy, S-hydroxyl	3.2	4.4×10^{10}	8.8	3.7×10^{6}
Δ^3-carene R- alkoxy, R-hydroxyl	4.0	1.5×10^{10}	8.0	2.7×10^{7}
Δ^3-carene S- alkoxy, R-hydroxyl	4.4	7.4×10^{9}	7.0	8.2×10^{7}

S10. Transition states and energetics for reaction R6 (bond scission in the keto-nitrooxy-alkyl radical formed in the Δ-carene + NO_3 system by reaction R5b)

The zero-point corrected ωB97X-D/aug-cc-pVTZ electronic energy barriers for the bond scission reactions of the second-generation alkyl radicals (keto-nitrooxy-alkyl radicals) formed in the Δ^3-carene + NO_3 system (**R6** in Scheme 2 of the main manuscript) are 6.15 kcal/mol and 6.43 kcal/mol for the R and S isomers, respectively. This corresponds to lowest energy single-conformer transition state theory (LC-TST) reaction rate constants of 3.3×10^8 s^{-1} and 1.1×10^8 s^{-1} for the two isomers, respectively. The barriers and rate constants are calculated based on ωB97X-D/aug-cc-pVTZ optimizations and frequency calculations on the lowest zero-point corrected electronic energy conformer of the reactant and transition state of the two isomers at the B3LYP/6-31+G(d) level of theory. The lowest-energy transition states for reaction **R6** are shown in Figure S7.

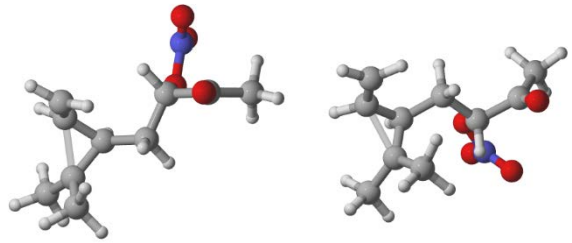

Figure S7. Lowest-energy transition state conformers for Reaction **R6** in Scheme 2 of the main manuscript. Right: R-isomer, left: S-isomer. Color coding as in Figure 1 & S1.

S11. Detailed description of experimental instrumentation

The FIXCIT chamber experiment described here is number 13, one of two "Competitive-HO_2 nitrate (NO_3) oxidation" experiments, described in the FIXCIT overview paper.[12] The instrumentation referred to in the main text and used to determine nitrooxy-hydroperoxide, pinonaldehyde, and organic aerosol yields is described below. N.B.: in order to achieve RO_2 + HO_2 dominated chemistry, it was essential to inject α-pinene slowly into the chamber containing NO_2, O_3, and HCHO. Rapid injection favors RO_2+ RO_2 chemistry because the NO_3 + α-pinene reaction is rapid. This is generally true for monoterpenes, which react very rapidly with NO_3.

Chamber Conditions

α-Pinene was injected by volume with a gas-tight syringe over 1.25 hours using a syringe pump. Due to large sampling flows from instruments during the FIXIT campaign,[12] the reported initial α-pinene concentration was corrected for chamber volume loss during the experiment set-up and α-pinene injection. α-Pinene will react with both NO_3 and O_3 under the experimental conditions used in this study. To estimate the branching ratio for the NO_3-RO_2 + HO_2 → NO_3-ROOH + O_2 channel, the fraction of α-pinene reacting with NO_3 needs to be estimated. This fraction (~70%) was estimated by assuming most NO_3 loss is due to reaction with α-pinene and therefore the fraction of α-pinene loss due to NO_3 chemistry is $P_{NO3}/(P_{NO3}+k_{O3+\alpha\text{-pinene}}[O_3][\alpha\text{-pinene}])$ where $P_{NO3} = k_{NO2+O3}[O_3][NO_2]$. We have used the recommended IUPAC rates for α-pinene loss via NO_3. IUPAC recommended rates were used for $k_{O3+\alpha\text{-pinene}}$ and k_{NO2+O3}. We note that the low observed organic aerosol yield is consistent with only a small contribution of O_3 + *α*-pinene chemistry, since the secondary organic aerosol (SOA) yield from that reaction has been shown to be large.[13-14] A time-series plot of key species from the experiment analyzed is shown in Figure S8.

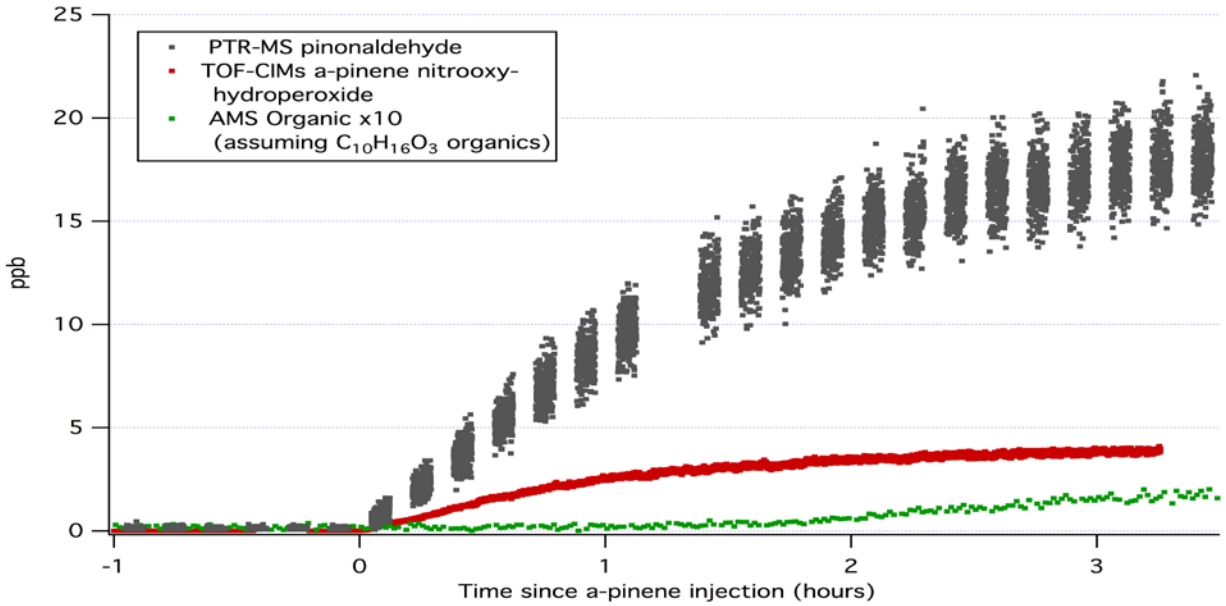

Figure S8. Time series of relevant product species from FIXCIT experiment #13, NO_3 + *α*-pinene under HO_2 dominated conditions. Total organic mass from the Aerosol Mass Spectrometer (AMS) has been converted to ppb, assuming an average molecular structure of $C_{10}H_{16}O_3$ (based on observed O:C ratio of ~ 0.25 in OA), and has been multiplied by 10 to put on the same scale.

Switchable reagent ion high-resolution time of flight mass spectrometer (SRI-ToFMS)

The gas phase volatile organic compounds (VOC) were measured with a proton transfer reaction time of flight mass spectrometer (PTR-TOF-MS 8000, Ionicon Analytik GmbH, Austria) equipped with switchable reagent ion (SRI) capability. Two ionization reagents (H_3O^+ and NO^+) were used and the data reported here was measured in H_3O^+ mode. For H_3O^+ mode, the ionization conditions in the drift tube were controlled by setting the drift voltage to 502 V, drift temperature to 60 °C and drift pressure to 2.3 mbar, resulting in an E/N value of 111 Td (with E being the electric field strength, and N the gas number density; 1 Td = 10^{-17} V cm^2). Each ionization mode ran for 10 min before switching to the other one. The m/z ion spectrum from 1.000 to 300.00 Th was processed using PTRwid.[15] For each experiment, the instrument was calibrated using an authentic VOC standard mixture (Apel-Riemer) containing compounds (including α-pinene) at concentrations certified at 5% accuracy. The standard was dynamically diluted with VOC-free air to concentrations in the low ppb range. The accuracy for reported α-pinene concentration in the chamber is expected to be better than 10%.

Pinonaldehyde is a challenging compound to measure because of its high fragmentation and lack of authentic standards. Wisthaler et al. and Lee et al. identified many ions related to pinonaldehyde.[16-17] Here, we applied a new approach, which takes into account m/z 151.1 (the most abundant pinonaldehyde fragment ion, and one without interferences) and applies a correction factor to account for the contribution from all remaining ions. The fraction of signal observed at m/z 151.1 was obtained from calibration on synthesized pure pinonaldehyde standard (>90% purity) over a wide range of E/N ratios. Pinonaldehyde concentration (c_{pinal}) are then obtained by multiplying concentration of m/z 151.1 ion ($c_{m151.1}$) by the fraction factor (ff, here 3.2) corresponding to the appropriate E/N ratio. Such approach should also work for low concentrations of pinonaldehyde.

$$C_{pinal} = ff * C_{m151.1} \quad \text{(S1)}$$

This approach results in an estimated 20% accuracy for the reported pinonaldehyde concentration. This uncertainty does not include the potential interference if nitrooxy hydroperoxide is converted to pinonaldehyde in the PTRMS, analogous to ISOPOOH rearrangement to MACR or MVK.[18] The extent to which this could occur in monoterpene-derived NO_3-ROOH vs isoprene-derived OH-ROOH is unknown.

Time of flight chemical ionization mass spectrometer (ToF-CIMS)

The gaseous nitrooxy hydroperoxide products of α-pinene oxidation were quantified with a time-of-flight (ToF) chemical ionization mass spectrometer (CIMS) using CF_3O^- as an ionization reagent.[19] The sample flow from the chamber was diluted with dry N_2 prior to mass spectrometry analysis. The dilution was accounted for in the analytical workup. The dry (RH < 5%) sensitivity of the ToF CIMS was calibrated for several compounds where the commercial or synthesized standards were available during the FIXCIT campaign (e.g., H_2O_2, HCOOH, peracetic acid (PAA), acetic acid (AA), hydroxyacetone (HAC), C_5 isoprene hydroxy nitrates (ISOPNs), isoprene dihydroxy epoxides (IEPOX), isoprene hydroxy hydroperoxide (ISOPOOH), etc.). The absolute calibrations were based on gravimetric or spectrometric techniques.

For the multifunctional products of α-pinene oxidation, where no analytical standards are available, a calibration factor was estimated from both GC-CIMS measurements and from calculated dipole moment and polarizability (Table S7).[20-21] The measurement uncertainty using this approach is estimated to be +-50%. Nitrooxy hydroperoxide is detected at m/z (-) 316 (i.e., analyte complexed with CF_3O^-). The ion-molecule collision rate relative to C_5 isoprene hydroxy nitrates (ISOPN, CF_3O^- cluster at m/z 232) is calculated to be 1.30, using the dipole moments and polarizabilities calculated by (average of tertiary-OOH isomers of the nitrooxy hydroperoxide of α-pinene: dipole=3.50 Debye; polarizibility=20.92 $Å^3$). Mass discrimination in the TOF is estimated, however, to reduce the sensitivity at m/z 316 25(+-15)% relative to m/z 232. Finally, using the GC-TOFCIMS[12], we find that only ~3% of the nitrooxy hydroperoxide CIMS signal is detected at fragmentation ions (the nitrooxy hydroperoxides are transmitted (~70%) through the GC -. There is still potential for systematic error if fragmentation yields unquantifiable anions (e.g CF_3O^-). The ToF-CIMS detected minimal formation of other organic nitrates (~1 ppb).

Aerosol mass spectrometer (AMS)

Aerosol chemical composition was measured with a high-resolution time-of-flight aerosol mass spectrometer (ToF-AMS, Aerodyne Research Inc.) operated in V mode (R ~ 2000 at m/z 200) and W mode (R ~ 3000 – 4000 at m/z 200). Ionization efficiency was calibrated using 350 nm diameter ammonium nitrate particles. IGOR Pro 6.31 (WaveMetrics, Inc.,) and the SQUIRREL v 1.51H and PIKA v 1.10H analysis toolkits were used to analyze AMS data. Total mass concentration of organic aerosol (μg m^{-3}) was calculated by summing the nitrate-equivalent masses of each high-resolution organic-associated ion from the V-mode data. Particles were sampled through a 130-cm Nafion drier (MD-110, Permapure LLC) at a flow rate of 0.084 L min^{-1}. Drying the particles may introduce particle or organic line losses in the drier tube and change the particle bounce characteristics on the AMS vaporizer plate. These perturbations may be corrected by applying a collection-efficiency (CE) factor. For these experiments, the CE of aerosol particles was determined by measuring the mass concentrations of organics, sulfate, and ammonium of the wet particles without the Nafion drier, assuming losses are negligible in this configuration, and comparing with measurements made through a drier. Using this method, a CE of 0.50 was determined for the FIXCIT campaign, and applied to all AMS measurements.

Calculated dipole moments and polarizabilities of α-pinene hydroperoxides for CIMS calibration

Values are calculated in Gaussian 09 using MMFF conformer sampling in Spartan'14. Both the dipole moments and polarizabilities are calculated as Boltzmann weighted averages over all conformers based on their zero-point corrected electronic energies at the B3LYP/cc-pVTZ level as used previously.[20] In the CIMS calibration we have used a dipole of 3.50 D and polarizability of 20.92 $Å^3$, corresponding to the isomer average of the main addition pathway. The values for the minor pathway to form the secondary radical are very similar.

Table S7. Calculated conformationally averaged dipole moments and polazibabilities for the hydroperoxide isomers. Calculated using zero-point corrected electronic energies of all conformers found with the B3LYP/aug-cc-pVTZ method and at 298.15 K.

Hydroperoxide isomer *Addition to form tertiary radical* 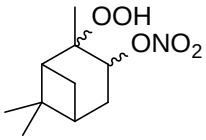	Dipole moment (D)	Polarizability ($Å^3$)
α-pinene R-hydroperoxide, S-nitrooxy	3.76	20.92
α-pinene S-hydroperoxide, S-nitrooxy	3.50	20.91
α-pinene R-hydroperoxide, R-nitrooxy	3.38	20.90
α-pinene S-hydroperoxide, R-nitrooxy	3.37	20.93
Isomer average	**3.50**	**20.92**
Hydroperoxide isomer *Addition to form secondary radical* 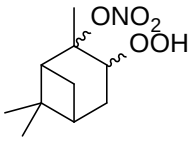	Dipole moment (D)	Polarizability ($Å^3$)
α-pinene R-hydroperoxide, S-nitrooxy	3.55	20.65
α-pinene S-hydroperoxide, S-nitrooxy	3.30	20.79
α-pinene R-hydroperoxide, R-nitrooxy	3.39	20.88
α-pinene S-hydroperoxide, R-nitrooxy	3.92	20.79
Isomer average	**3.54**	**20.78**

S12. Alkoxy bond breaking reactions in isoprene-derived nitrooxy alkoxy radicals

We have also studied the rates of the two different alkoxy bond breakings (similar to **R5a/b** in scheme 1 and 2 of the main manuscript) in two different nitrooxy alkoxy radicals derived from isoprene. The two differ only in the position of the nitrooxy group, one having it on a secondary carbon atom (sec-nitrooxy) and the other having it on a tertiary carbon atom (ter-nitrooxy). For both, the alkoxy radical can break either the bond to the $CONO_2$-group (left column in Figure S9) or to the COH-group, see Figure S9. The rates of these alkoxy bond breaking reactions have been calculated using MC-TST as described in Section S1. The reaction barriers have been calculated for the lowest energy (ωB97X-D/aug-cc-pVTZ zero-point corrected energy) conformers both at the ωB97X-D/aug-cc-pVTZ level and at the CCSD(T)-F12a/VTZ-F12//ωB97X-D/aug-cc-pVTZ level. All rates are without tunneling, as all imaginary frequencies below 400 cm^{-1} and are for the R,R isomer of the radicals. The barriers and rates are given in Tables S8 and S9.

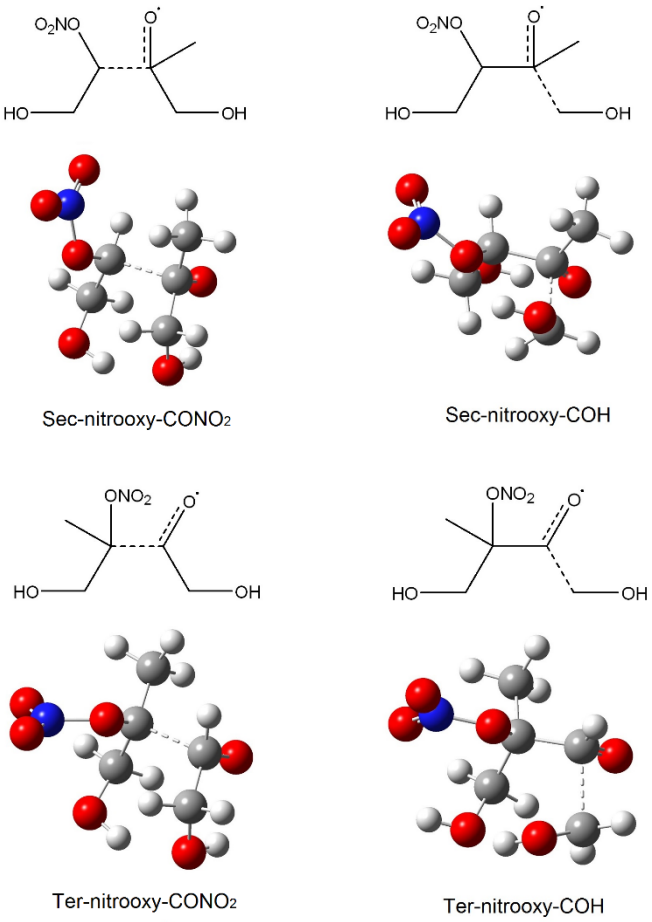

Figure S9. Schematic structures and lowest energy conformers (ωB97X-D/aug-cc-pVTZ zero-point corrected energy) of the four different transition states for the alkoxy bond breakings. Top row have the structures with the nitrooxy group on the secondary carbon, while the bottom row have the structures with the nitrooxy group on the tertiary carbon atom. Left column corresponds to breaking of the C-$CONO_2$ bond, while the right column corresponds to breaking of the C-COH bond.

Table S8. Calculated reaction barriers (zero-point corrected electronic energy difference between reactant and transition state) in kcal/mol. The barriers are calculated between the ωB97X-D/aug-cc-pVTZ lowest-energy conformer of each species. The electronic energies are at the two different levels of theory indicated and both use the ωB97X-D/aug-cc-pVTZ zero-point correction.

	ωB97X-D/aug-cc-pVTZ	CCSD(T)-F12a/VDZ-F12
Sec-nitrooxy-$CONO_2$	5.01	6.21
Sec-nitrooxy-COH	3.25	4.65
Ter-nitrooxy-$CONO_2$	5.73	6.14
Ter-nitrooxy-COH	5.41	6.54

Table S9. MC-TST calculated reaction rate constants (s^{-1}) for the two different alkoxy ring breaking reactions of the two nitrooxy alkoxy systems. All partition functions and relative energies between conformers are calculated at the ωB97X-D/aug-cc-pVTZ, while the reaction barrier are those in Table S8.

	ωB97X-D/aug-cc-pVTZ	CCSD(T)-F12a/VDZ-F12
Sec-nitrooxy-$CONO_2$	4.1×10^{8}	5.4×10^{7}
Sec-nitrooxy-COH	2.5×10^{10}	2.4×10^{9}
Ter-nitrooxy-$CONO_2$	1.6×10^{8}	7.8×10^{7}
Ter-nitrooxy-COH	3.0×10^{8}	4.4×10^{7}

In table S9, we show that the rate of the two alkoxy bond breakings are comparable in the structures with the tertiary nitrooxy, while breaking of the C-COH bond is significantly preferred, by about a factor of ~50, in the structure with the secondary nitrooxy.

References in the Supporting Information

1. Møller, K. H.; Otkjær, R. V.; Hyttinen, N.; Kurtén, T.; Kjaergaard, H. G. Cost-Effective Implementation of Multiconformer Transition State Theory for Peroxy Radical Hydrogen Shift Reactions. *J. Phys. Chem. A* **2016,** *120*, 10072-10087.
2. Vereecken, L.; Peeters, J. The 1,5-H-shift in 1-butoxy: A Case Study in the Rigorous Implementation of Transition State Theory for a Multirotamer System. *J. Chem. Phys.* **2003,** *119*, 5159-5170.
3. *Spartan'14*, Wavefunction, Inc., Irvine, CA: 2014.
4. Frisch, M. J.; Trucks, G. W.; Schlegel, H. B.; Scuseria, G. E.; Robb, M. A.; Cheeseman, J. R.; Scalmani, G.; Barone, V.; Mennucci, B.; Petersson, G. A.; Nakatsuji, H.; Caricato, M.; Li, X.; Hratchian, H. P.; Izmaylov, A. F.; Bloino, J.; Zheng, G.; Sonnenberg, J. L.; Hada, M.; Ehara, M.; Toyota, K.; Fukuda, R.; Hasegawa, J.; Ishida, M.; Nakajima, T.; Honda, Y.; Kitao, O.; Nakai, H.; Vreven, T.; Montgomery Jr., J. A.; Peralta, J. E.; Ogliaro, F.; Bearpark, M. J.; Heyd, J.; Brothers, E. N.; Kudin, K. N.; Staroverov, V. N.; Kobayashi, R.; Normand, J.; Raghavachari, K.; Rendell, A. P.; Burant, J. C.; Iyengar, S. S.; Tomasi, J.; Cossi, M.; Rega, N.; Millam, N. J.; Klene, M.; Knox, J. E.; Cross, J. B.; Bakken, V.; Adamo, C.; Jaramillo, J.; Gomperts, R.; Stratmann, R. E.; Yazyev, O.; Austin, A. J.; Cammi, R.; Pomelli, C.; Ochterski, J. W.; Martin, R. L.; Morokuma, K.; Zakrzewski, V. G.; Voth, G. A.; Salvador, P.; Dannenberg, J. J.; Dapprich, S.; Daniels, A. D.; Farkas, Ö.; Foresman, J. B.; Ortiz, J. V.; Cioslowski, J.; Fox, D. J. *Gaussian 09, Revision D.01*, Gaussian, Inc.: Wallingford, CT, USA, 2009.
5. Peterson, K. A.; Adler, T. B.; Werner, H.-J. Systematically Convergent Basis Sets for Explicitly Correlated Wavefunctions: The Atoms H, He, B−Ne, and Al−Ar. . *J. Chem. Phys.* **2008,** *128*, 084102.
6. Glowacki, D. R.; Liang, C.-H.; Morley, C.; Pilling, M. J.; Robertson, S. H. MESMER: An Open-Source Master Equation Solver for Multi-Energy Well Reactions. *J. Phys. Chem. A* **2012,** *116*, 9545-9560.
7. Cuadros, F.; Cachadiña, I.; Ahumada, W. Determination of Lennard-Jones interaction parameters using a new procedure. *Mol. Eng.* **1996,** *6*, 319-325.
8. Kurtén, T.; Rissanen, M. P.; Mackeprang, K.; Thornton, J. A.; Hyttinen, N.; Jørgensen, S.; Ehn, M.; Kjaergaard, H. G. Computational Study of Hydrogen Shifts and Ring-Opening Mechanisms in α-Pinene Ozonolysis Products. *J. Phys. Chem. A* **2015,** *119*, 11366-11375.
9. Penner, A. P.; Forst, W. Analytic Solution of Relaxation in a System with Exponential Transition Probabilities. *J. Chem. Phys.* **1977,** *67*, 5296-5307.
10. Hyttinen, N.; Knap, H. C.; Rissanen, M. P.; Jørgensen, S.; Kjaergaard, H. G.; Kurtén, T. Unimolecular HO2Loss from Peroxy Radicals Formed in Autoxidation Is Unlikely under Atmospheric Conditions. *J. Phys. Chem. A* **2016,** *120*, 3588-3595.
11. Atkinson, R.; Baulch, D. L.; Cox, R. A.; Crowley, J. N.; Hampson, R. F.; Hynes, R. G.; Jenkin, M. E.; Rossi, M. J.; Troe, J.; Subcommittee, I. Evaluated Kinetic and Photochemical Data for Atmospheric Chemistry: Volume II - Gas Phase Reactions of Organic Species. *Atmos. Chem. Phys.* **2006,** *6*, 3625-4055.
12. Nguyen, T. B.; Crounse, J. D.; Schwantes, R. H.; Teng, A. P.; Bates, K. H.; Zhang, X.; St. Clair, J. M.; Brune, W. H.; Tyndall, G. S.; Keutsch, F. N.; Seinfeld, J. H.; Wennberg, P. O. Overview of the Focused Isoprene eXperiment at the California Institute of Technology (FIXCIT): Mechanistic Chamber Studies on the Oxidation of Biogenic Compounds. *Atmos. Chem. Phys.* **2014,** *14*, 13531-13549.

13. Nah, T.; McVay, R. C.; Zhang, X.; Boyd, C. M.; Seinfeld, J. H.; Ng, N. L. Influence of Seed Aerosol Surface Area and Oxidation Rate on Vapor Wall Deposition and SOA Mass Yields: A Case Study with α-Pinene Ozonolysis. *Atmos. Chem. Phys.* **2016,** *16*, 9361-9379.
14. Shilling, J. E.; Chen, Q.; King, S. M.; Rosenoern, T.; Kroll, J. H.; Worsnop, D. R.; McKinney, K. A.; Martin, S. T. Particle Mass Yield in Secondary Organic Aerosol Formed by the Dark Ozonolysis of α-Pinene. *Atmos. Chem. Phys.* **2008,** *8*, 2073-2088.
15. Holzinger, R. PTRwid: A New Widget Tool for Processing PTR-TOF-MS Data. *Atmos. Meas. Tech.* **2015,** *8*, 3903-3922.
16. Wisthaler, A.; Jensen, N. R.; Winterhalter, R.; Lindinger, W.; Hjorth, J. Measurements of Acetone and Other Gas Phase Product Yields from the OH-Initiated Oxidation of Terpenes by Proton-Transfer-Reaction Mass Spectrometry (PTR-MS). *Atmos. Environ.* **2001,** *35*, 6181-6191.
17. Lee, A.; Goldstein, A. H.; Keywood, M. D.; Gao, S.; Varutbangkul, V.; Bahreini, R.; Ng, N. L.; Flagan, R. C.; Seinfeld, J. H. Gas-Phase Products and Secondary Aerosol Yields from the Ozonolysis of Ten Different Terpenes. *J. Geophys. Res. - Atmos.* **2006,** *111*, D07302.
18. Rivera-Rios, J. C.; Nguyen, T. B.; Crounse, J. D.; Jud, W.; St. Clair, J. M.; Mikoviny, T.; Gilman, J. B.; Lerner, B. M.; Kaiser, J. B.; de Gouw, J.; Wisthaler, A.; Hansel, A.; Wennberg, P. O.; Seinfeld, J. H.; Keutsch, F. N. Conversion of Hydroperoxides to Carbonyls in Field and Laboratory Instrumentation: Observational Bias in Diagnosing Pristine versus Anthropogenically-Controlled Atmospheric Chemistry. *Geophys. Res. Lett.* **2014,** *41*, 8645-8651.
19. Crounse, J. D.; McKinney, K. A.; Kwan, A. J.; Wennberg, P. O. Measurement of Gas-Phase Hydroperoxides by Chemical Ionization Mass Spectrometry. *Anal. Chem.* **2006,** *78*, 6726-6732.
20. Garden, A. L.; Paulot, F.; Crounse, J. D.; Maxwell-Cameron, I. J.; Wennberg, P. O.; Kjaergaard, H. G. Calculation of Conformationally Weighted Dipole Moments Useful in Ion–Molecule Collision Rate Estimates. *Chem. Phys. Lett.* **2009,** *474*, 45-50.
21. Su, T.; Chesnavich, W. J. Parametrization of the Ion–Polar Molecule Collision Rate Constant by Trajectory Calculations. *J. Chem. Phys.* **1982,** *76*, 5183-5185.